Coherent signals between the RAPID array and satellite altimetry

Zoltán B. Szűts and Jochem Marotzke
Max-Planck-Institut für Meteorologie
Bundesstraße 53, 20146 Hamburg, Germany.
zoltan.szuts@zmaw.de

1. INTRODUCTION

The RAPID array uses standard observational techniques — moored instruments that measure conductivity, temperature and pressure, as well as bottom pressure recorders — to measure density and pressure gradients across the North Atlantic, from which one can readily calculate the basin overturning circulation [1] and heat transport [2]. Although straightforward to implement, it is less obvious how to describe the observed low-frequency basin-wide signals in terms of specific dynamic processes. We approach this goal by decomposing full-depth observations in terms of vertical modes, which are then compared and contrasted with sea surface height (SSH) from altimetry.

More specifically, we investigate how well SSH can be used to reconstruct 1) full water-column density perturbations, 2) geostrophic transport fluctuations between moorings, and 3) the basin-wide overturning signal.

2. METHOD

The RAPID array is located along 26.5°N in the North Atlantic and has been operational since 2004. There are five full-depth moorings instrumented with typically 14 (range of 11–24) microcats which are redeployed yearly: WB2, WB3, and WB5, which are located 25, 50, and 500 km east of the Bahamas; Marwest, which is on the western flank of the Mid-Atlantic Ridge; and EB1, which is located 1250 km west of the North African coast. In this report we focus solely on these five full-depth moorings.

In the standard processing for the RAPID project [3], vertical profiles of temperature and salinity are generated by integrating climatological gradients vertically between sensors. Each depth level is low-pass filtered with a 2-day cut-off to remove tidal and inertial signals.

Here we generate continuous vertical profiles by fitting vertical modal structure to the discrete observations. This method is an alternative way to interpolate between sensors and to extrapolate to the surface, in addition to providing a dynamical basis for relating overturning circulation to sea surface expressions.

The steps to calculate wave perturbations are as follows: 1) density is calculated from the gridded temperature and salinity profiles, 2) the density is vertically integrated to obtain a pressure perturbation [4], 3) the pressure perturbations on constant depth-levels are calculated by extracting values at the median sensor depths, and 4) the pressure perturbations are de-meaned once more, and 5) dividing by the average density ρ_0 yields the reduced pressure perturbation.

Vertical modes arise from the equations of motion by performing separation of variables for the vertical dimension [5, 6]. The vertical modes are calculated from climatological profiles assuming a flat-bottomed and motionless ocean, and the structure of reduced pressure is the same as for horizontal velocities. For all moorings the first 8 modes (the barotropic plus the first 7 baroclinic modes) are fit to the reduced pressure perturbations with a minimum variance inversion called the Gauss-Markov inversion [7].

Three data sets are used here: the standard RAPID gridded geopotential anomalies ϕ (denoted "standard"); reconstructed reduced density perturbations p' based on vertical modes and mode amplitudes from the mode-fitting described above (denoted "reconstructed"), which are equivalent to geopotential anomaly perturbations; and scaled SSH $g\eta$ obtained from AVISO by interpolating the 7-day gridded product DT-MADT (Delayed Time Mean Absolute Dynamic Topography) onto the RAPID transect. All quantities have units of $\mathrm{m^2\,s^{-2}}$. The transports calculated below have integral time scales of roughly 25 days, which results in 50 degrees of freedom for 3.5 years of observations.

The reconstructed perturbations are done either using only the first baroclinic mode (BC1 reconstruction), or else using the barotropic plus 7 baroclinic modes (full-mode reconstruction). For comparing SSH with ϕ or p', we evaluate the latter two properties at a depth of 200 m to avoid surface effects [8]. For correlations with SSH, ϕ and p' are low-pass filtered with a cut-off frequency of 7 days to remove high-frequency variance not present in the altimetric product.

3. RESULTS

At first we consider each mooring in isolation, then the geopotential differences and transports between each mooring, and finally the basin-wide transport.

The first check on our method is whether the reconstructed p' values agree with the fluctuations in the original signal ϕ. At each station, the full-mode reconstruction recovers 80–98% of the variance (r^2) of the standard ϕ at 200 m and the rms amplitudes are the same size. Down to 3500 m the full-mode reconstructions recovers a similar fractions of the variance, except at EB1 where the correlation decreases below 1000 m. Although the BC1 reconstruction recovers 70–98% (r^2) of the variance in ϕ at 200 m, the correlation is only high in the upper 1000–1500 meters, below which the correlation changes sign as expected and decreases towards the bottom.

The variance contained in the modes and their correlation are shown in Figure 1. The near-surface standard deviations of ϕ and the BC1 reconstructions increase away from the boundaries, and SSH is most-correlated with ϕ near the surface. In general the BC1 reconstruction (at 200 m) is as well correlated with SSH as is ϕ (Figure 1e), but there's a large increase in correlation away from the boundaries.

A second way to evaluate the modal decomposition is by considering how well it recovers gradients (and thus transports) between adjacent moorings. In the vertical, the full-mode reconstruction is well correlated in the upper 3000 m ($r^2 = 0.65$ between WB2 and WB3, otherwise $> 90\%$ for the other station pairs), while the BC1 reconstruction is only well-correlated in the upper 1000 m. Inclusion of bottom pressure makes little difference for the correlations presented here. The correlation of sea surface slope with gradients of ϕ or of the full-mode or BC1 reconstructions at 200 db increases from WB2/WB3 (0.57) to WB3/WB5 (0.83), to WB5/Marwest (0.86), and then decreases slightly at Marwest/EB1 (0.71). The rms amplitudes of $g\Delta\eta$, $\Delta\phi$, and $\Delta p'$ are similar in magnitude.

The transport from ϕ between two moorings (T_ϕ) is calculated by vertically integrating the geostrophic velocity between stations and multiplying by the horizontal distance. For the transport from p' ($T_{p'}$), the time-averaged vertical structure of ϕ needs to be added back to the time-perturbations before integrating vertically. For reconstructing transport from SSH ($T_{\rm SSH}$), the simplest method is to expand the vertical structure at each mooring location with the first baroclinic mode and then calculate the geostrophic transport between stations. In practice, the standard deviations from this method are much larger than expected (factors of 10–100). Instead, SSH anomalies in a line between stations are expanded over the full water column with the first baroclinic mode, and then this field is integrated to obtain transport. The results for each station pair is shown in Figure 2.

The full-mode transport $T_{p'}$ (not shown) recovers nearly all of the variance ($r^2 = 0.9$–1), except at WB2 where significantly less is recovered ($r^2 = 0.62$). The full modal decomposition thus is able to recover the dominant transport signals except at WB2. If only the first baroclinic mode is used in the reconstruction (Figure 2), however, the common variance reduces to 0.6–0.9 (but 0.5 at WB2).

Generally, the SSH-derived transport $T_{\rm SSH}$ is poorly correlated with T_ϕ ($r = 0.2$–0.7), and the rms amplitude of $T_{\rm SSH}$ is much smaller than T_ϕ (13–50%). Despite the reduced amplitude variance in the BC1 $T_{p'}$, this reconstruction has a slightly larger correlation with SSH (0.3-0.8).

Now we consider the third quantity: the basin-wide transport. Because vertical modes are not appropriate for describing changes along a sloping boundary, we terminate our calculation at EB1 instead of using the density profile along the boundary as done by [9]. The transport from the basin-wide full-mode reconstruction $T_{p'}$ recovers $r^2 = 0.79$ of the variance of T_ϕ, but its correlation with SSH only recovers $r^2 = 0.34$ of the variance (0.22 for T_ϕ). Surprisingly, the BC1 reconstruction recovers significantly more of the variance ($r^2 = 0.55$), despite its standard deviation being smaller than that of T_ϕ.

4. DISCUSSION

Although it is expected that SSH is predominantly set by the first baroclinic mode [10], the long-duration and full-watercolumn measurements made by RAPID allow this statement to be examined in greater detail for the temporal fluctuations.

From a local analysis at each mooring, the BC1 vertical mode is able to recover over 80% of the variance above the thermocline at any one station in the ocean interior. Aside from the stations close to the boundaries (WB2, WB3 and EB1), the first mode also captures most of the vertical variance. This agreement is not unexpected, but examining where it fails provides further insight.

The dynamics close to the boundaries are not well captured by the simple modes chosen here, despite the BC1 mode at WB2 extracting a signal more coherent with SSH. Better attribution of the dynamics may result from using more appropriate modal structures — whether by making different assumptions (the presence of mean velocities, [11]; including other non-linearities [12]; surface-intensified modes with varying horizontal wavenumbers, [13]) or with empirical statistics (e.g. the gravest empirical mode, [14]).

The transports at WB2 and EB1 are quite different, however: the former contains large high frequency components (periods of 2-20 days), while the latter contains almost no energy at these periods. While one might expect wind-forced modes to be important at the eastern boundary [15], how or whether this mechanism is responsible for the annual signal is not yet clear. In contrast, the western boundary is not only influenced by strong deep and surface currents, but also by westward traveling eddies that hit the continental margin and generate fast boboundary responses. Although the eddy variance decreases markedly at WB2 compared with WB5 [8], the actual dissipation and reflection mechanisms of these signals is not yet characterized. To the extent that processes with multiple vertical structures are present, then there is only hope for recovering from SSH the variance associated with the dominant process, and additional dynamic structures merely reduce the amount of variance recoverable.

In the interior, there is clear compensation west of the Mid-Atlantic Ridge on either side of WB5 from the anti-correlation of transport between WB3/WB5 and WB5/Marwest. This compensation may simply be eddies passing by WB5 or Marwest, or it may reflect larger scale fluctuations of the subtropical gyre.

When the integration domain spans the deep basin, how-

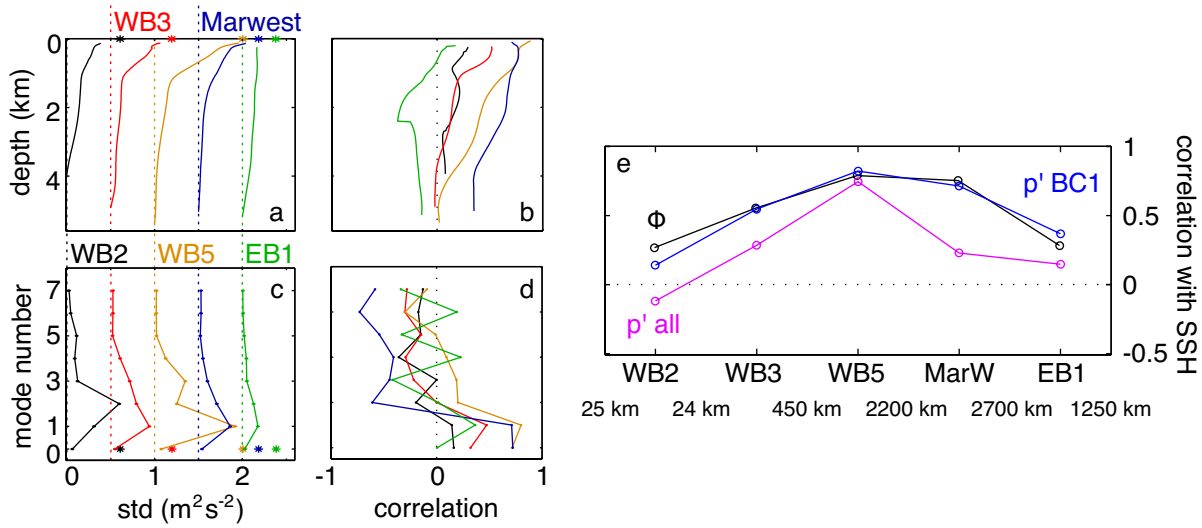

Figure 1: *Local analysis at each mooring. In depth-coordinates: (a) std of ϕ (lines) and $g\eta'$ (*), and (b) correlation of $\phi(z=200\,m)$ with $g\eta'$. In mode-coordinates: (c) std of P_i (lines) and $g\eta'$ (*), and (d) correlation of $P_iF_i(z=200\,m)$ with $g\eta'$. Standard deviations are offset horizontally by $0.5\,m^2\,s^{-2}$. (e) Correlation between SSH and one of ϕ (black), p'/ρ_0 using $i=0,\ldots,7$ (magenta), or p'/ρ_0 using $i=1$ (BC1) (blue), all evaluated at $z=200\,m$. The distances between the moorings are also given.*

ever, the non-resolved dynamics dominate such that the weak correlation between SSH and internal signals at the boundaries prevents accurate recovery of the overturning circulation. The BC1 reconstruction does an unexpectedly good job of recovering the transport signal ($r^2=0.5$), but only half of this ($r^2=0.25$) can be extracted from SSH.

Although this modal decomposition approach will be refined further, it is surprising how well the simple dynamics used here are able to extract mid-ocean signals from SSH.

5. REFERENCES

1. Cunningham, S.A., T. Kanzow, D. Rayner, M.O. Baringer, W.E. Johns, J. Marotzke, H.R. Longworth, E.M. Grant, J.J-M. Hirschi, L.M. Beal, C.S. Meinen, and H.L. Bryden. (2007). Temporal variability of the Atlantic meridional overturning circulation at 26.5 degrees N. *Science*, **317**(5840), 935–938.

2. Johns, W.E., T. Kanzow, S.A. Cunningham, M.O. Baringer, H.L. Bryden, and C.S. Meinen. (2009). Heat transport across the rapid array. *in prep.*.

3. Kanzow, T., S.A. Cunningham, D. Rayner, J.J-M. Hirschi, W.E. Johns, M.O. Baringer, H.L. Bryden, L.M. Beal, C.S. Meinen, and J. Marotzke. (2007). Observed flow compensation associated with the MOC at 26.5 degrees N in the Atlantic. *Science*, **317**(5840), 938–941.

4. Kunze, E.,L.K. Rosenfeld, G.S. Carter, and M.C. Gregg. (2002). Internal waves in Monterey Submarine Canyon. *J. Phys. Ocean.*, **32**, 1890–1913.

5. Gill, A.E. (1982). *Atmosphere-Ocean Dynamics*, volume 30 of *International Geophysics Series*, Academic Press, San Diego, CA, USA.

6. Wunsch, C. and D. Stammer. (1997). Atmospheric loading and the oceanic "inverted barometer" effect. *Reviews of Geophysics*, **35**(1), 79–107.

7. Wunsch, C. (1996). *The Ocean Circulation Inverse Problem*, Cambridge University Press, Cambridge, United Kingdom.

8. Kanzow, T., H.L. Johnson, D.P. Marshall, S.A. Cunningham, J.J-M. Hirschi, A. Mujahid, H.L. Bryden, and W.E. Johns. (2009). Basin-wide integrated volumne transports in an eddy-filled ocean. *J. Phys. Ocean.: in press*.

9. Kanzow, T., S.A. Cunningham, W.E. Johns, J.J-M. Hirschi, J. Marotzke, M.O. Baringer, C.S. Meinen, M.P. Chidichimo, C. Atkinson, L.M. Beal, H.L. Bryden, and J. Collins. (2009). On the seasonal variability of the Atlantic meridional overturning circulation at 26.5°N. *submitt. to J. Climate*.

10. Stammer, D. (1997). Global characteristics of ocean variability estimated from regional TOPEX/POSEIDON altimeter measurements. *J. Phys. Ocean.*, **27**, 1743–1769.

11. Killworth, P.D., D.B. Chelton, and R.A. de Szoeke. (1997). The speed of observed and theoretical long extratropical planetary waves. *J. Phys. Ocean.*, **27**, 1946–1966.

12. Chelton, D.B., R.A. deSzoeke, M.G. Schlax, K. El Naggar, and N. Siwertz. (1998). Geographic variability of the first baroclinic Rossby radius of deformation. *J. Phys. Ocean.*, **28**, 433–460.

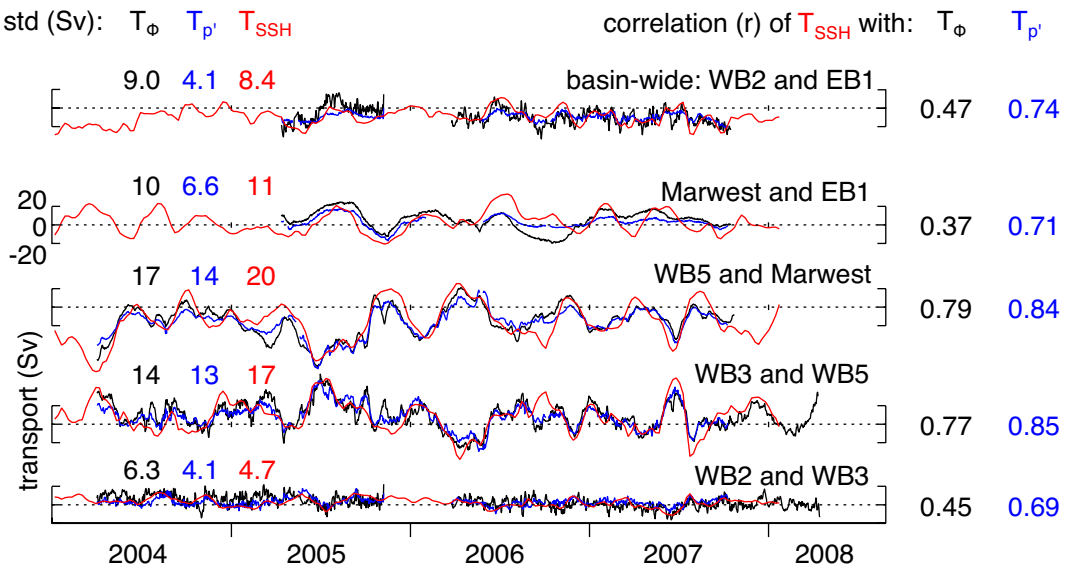

Figure 2: *The transport between the indicated station pairs for T_ϕ (black), $T_{p'}$ (blue), and T_{SSH} (red). At top is the basin-wide transport. The right two columns of numbers are the correlation (r) between T_{SSH} and either T_ϕ or $T_{p'}$, while the left three columns show the standard deviations for each of the transport calculations.*

13. Lapeyre, G. (2009). What vertical mode does the altimeter reflect? on the decomposition in baroclinic modes and on a surface-trapped mode. *J. Phys. Ocean.: in press*.

14. Watts, D.R., C. Sun, and S.R. Rintoul. (2001). A two-dimensional Gravest Empirical Mode determined from hydrographic observations in the Subantarctic Front. *J. Phys. Ocean.*, **31**, 2186–2209.

15. Chidichimo, M.P, T. Kanzow, S.A. Cunningham, W.E. Johns, and J. Marotzke. (2009). The contribution of eastern-boundary density variations to the Atlantic meridional overturning circulation at 26.5°N. *submitt. to Ocean Dynamics Disc.*